(6) Electrocatalysis for ORR/OER

1. High overpotential for ORR/OER

In acidic sol'n

$0.5O_2 + 2H^+ + 2e^- \leftrightarrow H_2O$ $\quad E_{rev(O2/H2O)} = 1.23$ V vs SHE

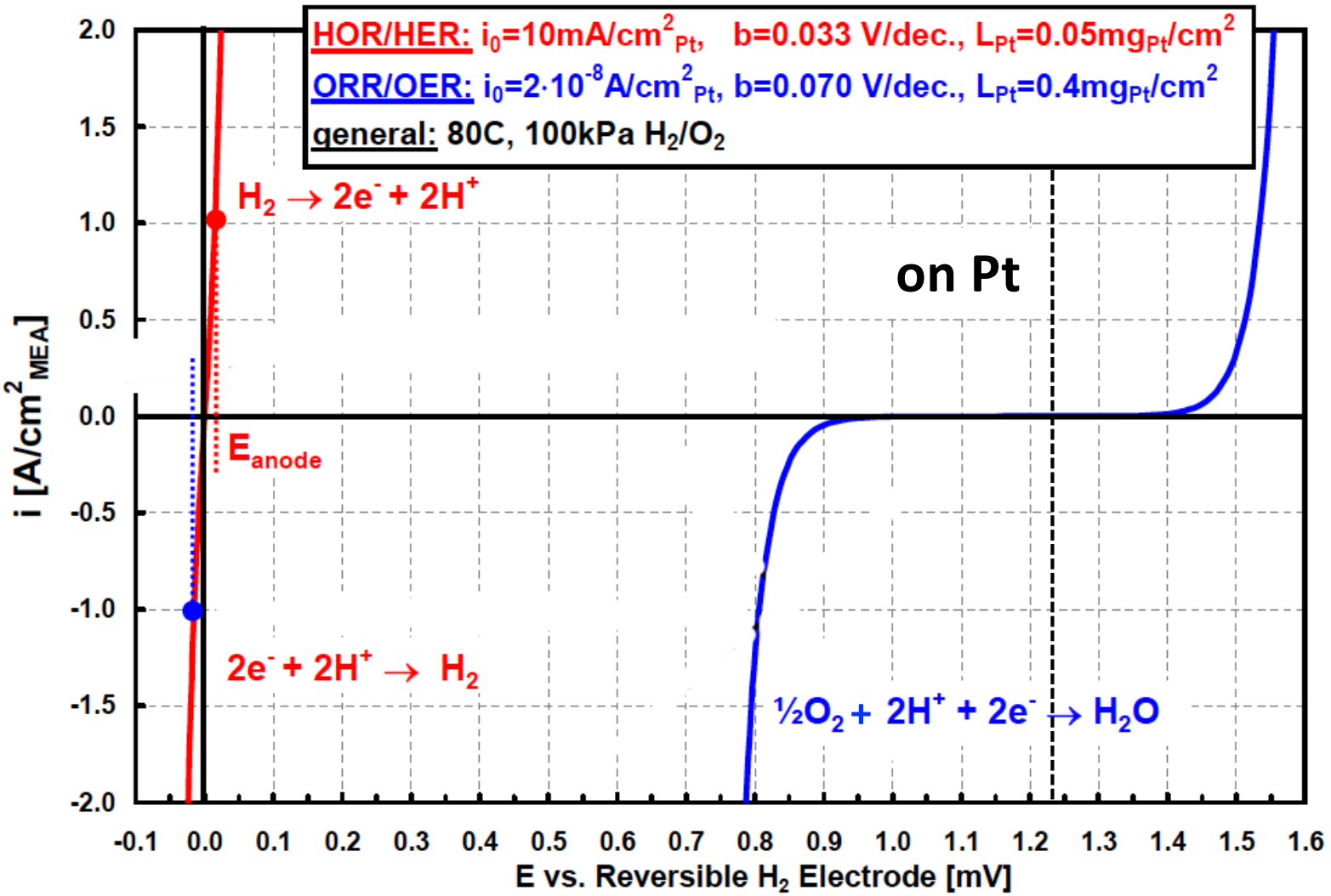

2. Molecular oxygen

Molecular orbital diagram for O_2

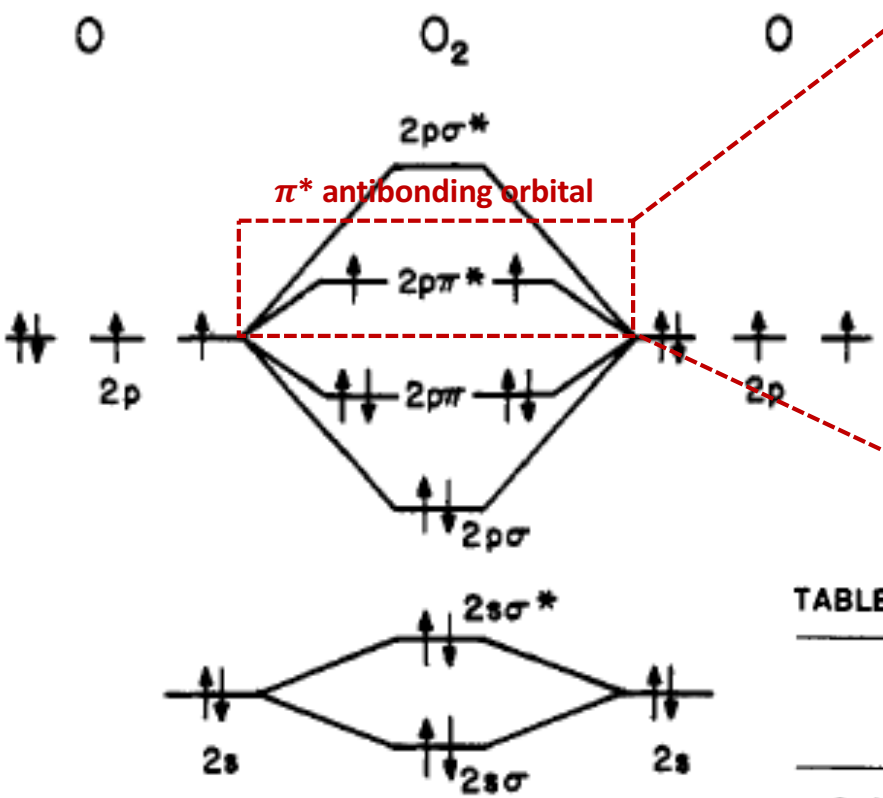

$(2s^2 2p^4)$

π^* orbital occupancy and energies of the first two electronically excited states of O_2.

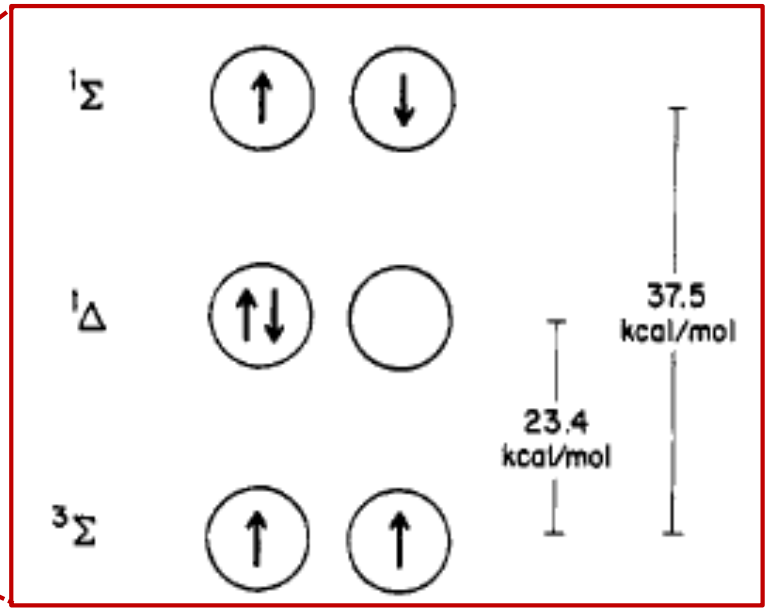

TABLE I. Inorganic Compounds of Dioxygen

	Example compd	O–O, Å[a]	Bond energy,[b] kcal/mol	Bond order
O_2^+	O_2PtF_6	1.12		2.5
O_2		1.21	118	2
O_2^- (superoxide)	KO_2	1.28		1.5
O_2^{2-} (peroxide)	H_2O_2	1.49	35	1

[a] F. A. Cotton and G. Wilkinson, "Advanced Inorganic Chemistry," 2nd ed, Interscience, New York, N. Y., 1966, p 333. [b] Reference 13.

Chem. Revs. **1973**, *73*, 235-245.

3. O_2 adsorption on metal catalyst

Relative energies of O_2 and metal bonding orbitals

	O_2	Metal (single atom)
1 σ bond:	π orbital →	*s*, *p*, and *d* orbital
2 π bonds:	π^* orbital ←	*d* orbital

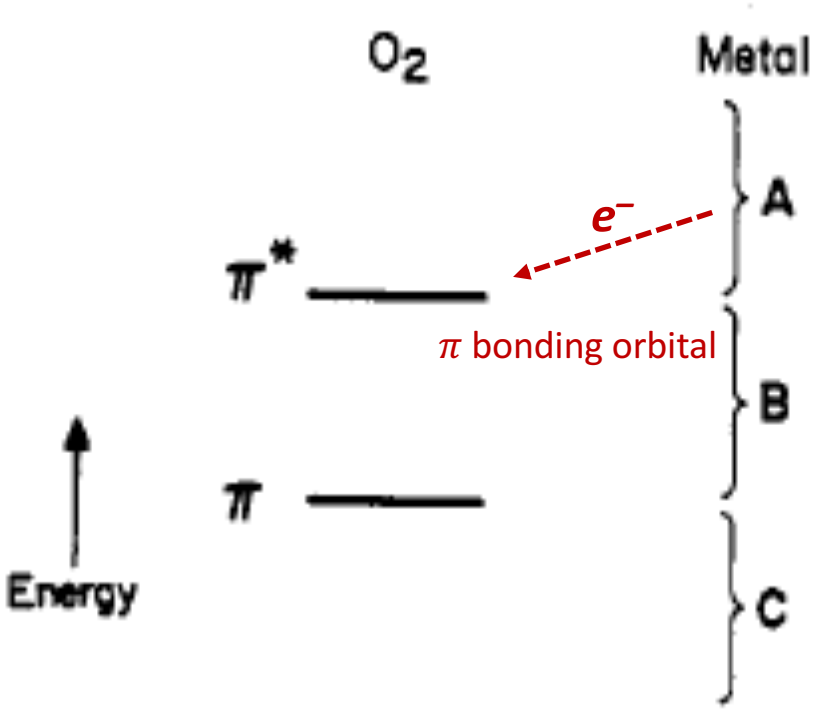

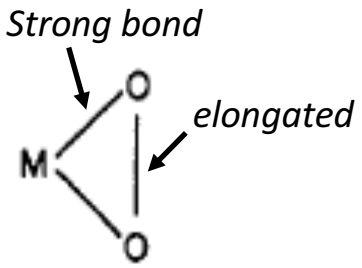

→ **O_2 dissociation**

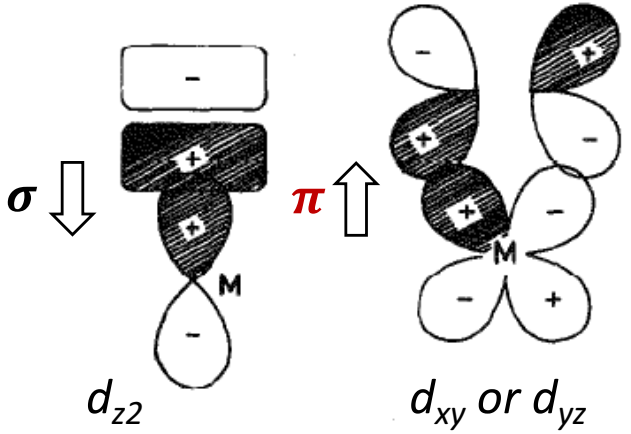

Chem. Revs. **1973**, *73*, 235-245.
Coord. Chem. Rev. **1992**, *119*, 89-136.

	side-on	*end-on*	*bridge*	*trans*
Model:	**Griffiths**	**Pauling**	**Yeager**	

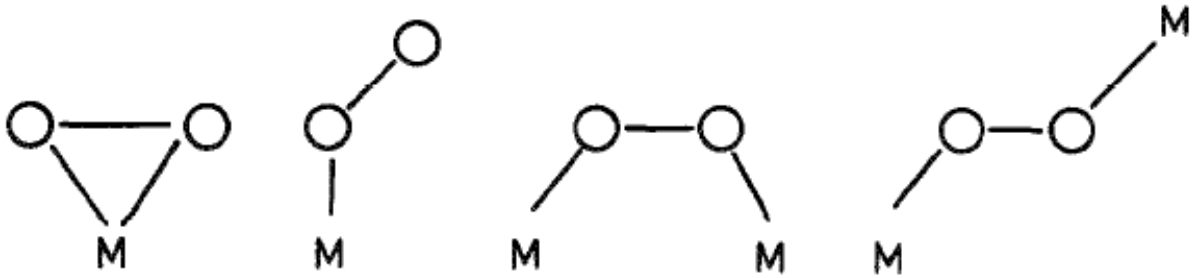

Some organometallic complex

Noble metal
Less H_2O_2 formation

Dimeric cobalt dioxygen complex

Phthalocyanine

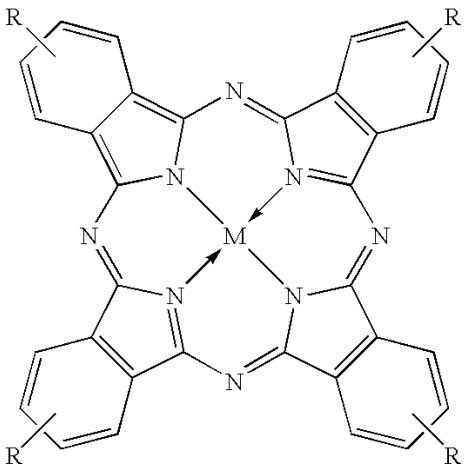

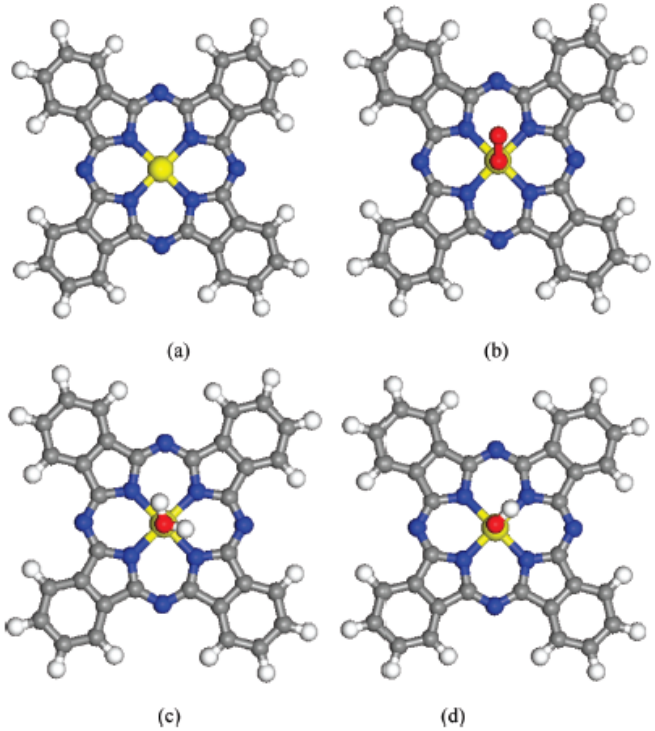

Figure 7. Optimized lowest energy structure of (a) isolated FePc or CoPc catalyst molecules, (b) O_2 adsorbed on FePc or CoPc, (c) H_2O adsorbed on FePc or CoPc, and (d) OH adsorbed on FePc or CoPc. The central yellow ball represents a metal Fe or Co atom, blue balls represent N atoms, gray balls represent C atoms, and light white balls represent H atoms.

Coord. Chem. Rev. **1992**, *119*, 89-136.
J. Phys. Chem. C **2009**, *113*, 20689-20697.

side-on

bridge

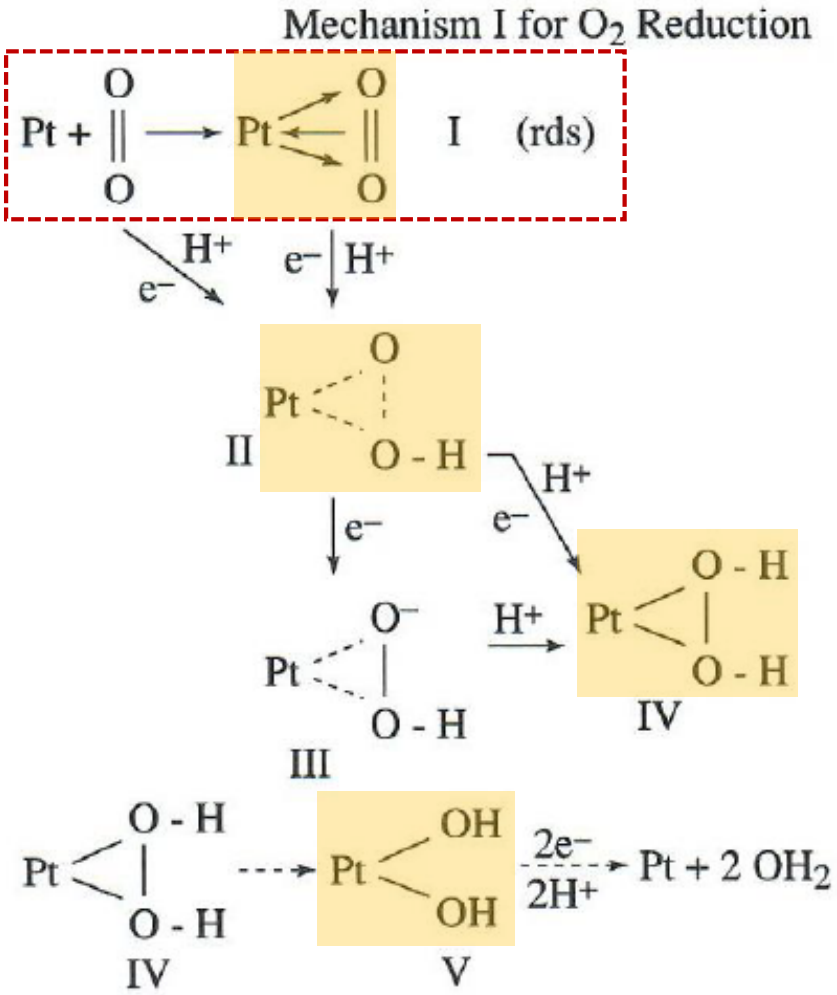

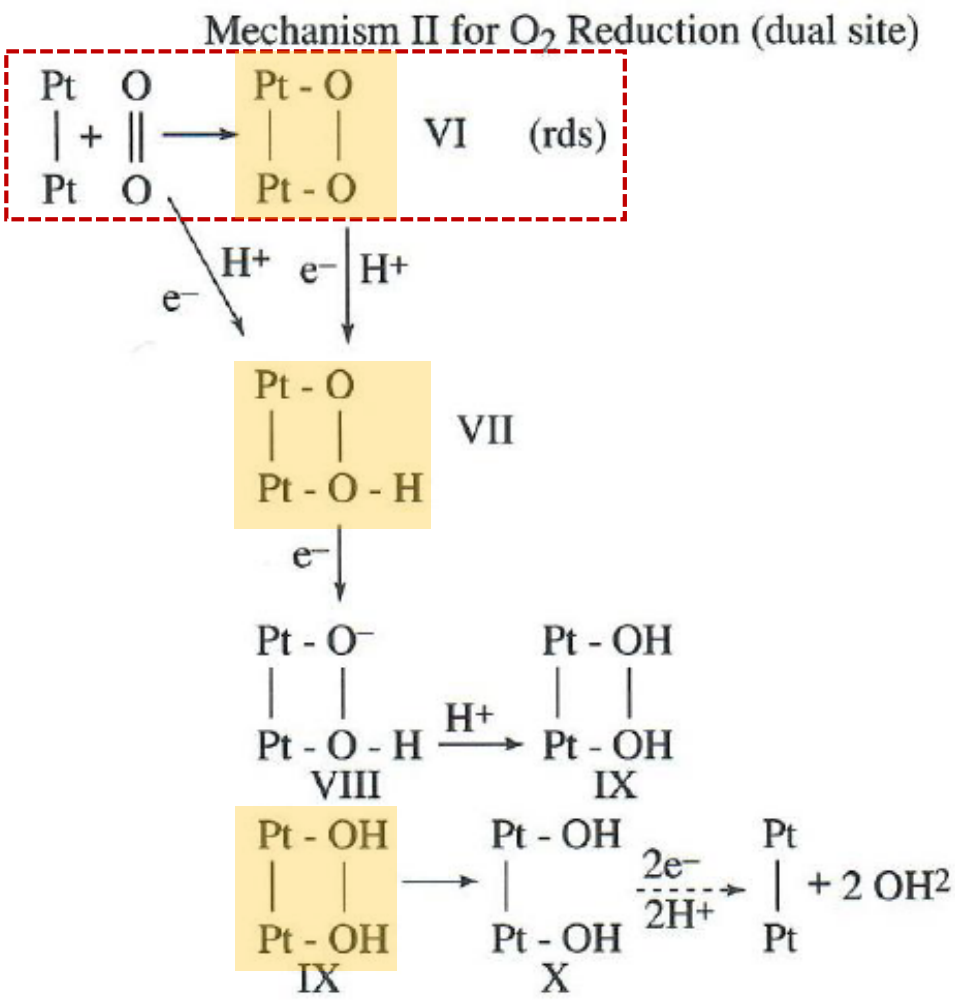

$O_2 \rightarrow O_2^- \rightarrow O_2^{2-} \rightarrow$ O-O bond breaking $\rightarrow$ O

Bond order: 2 1.5 1 0

Electrocatalysis, Wiley-VCH

Metal film (surface)

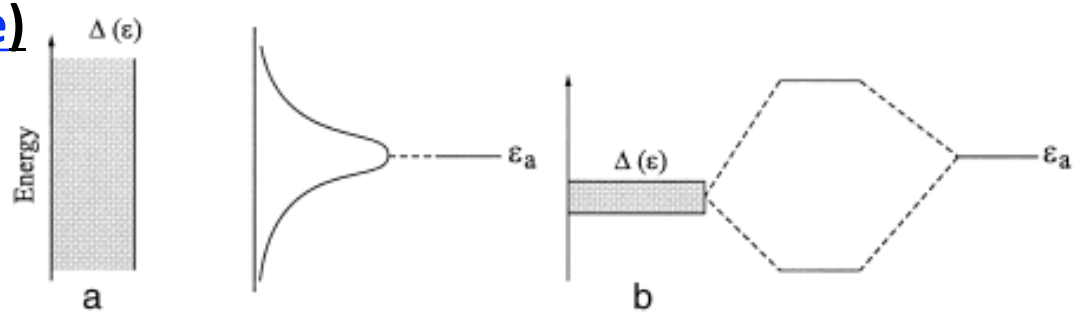

FIG. 3. The local density of states at an adsorbate in two limiting cases: (a) for a broad surface band; (b) for a narrow metal band. Case a corresponds to the interaction with a metal *s* band and case b is representative of the interaction with a transition metal *d* band.

Similar concept for adsorbent of C, O, N, H, F, S, and Cl to **M**

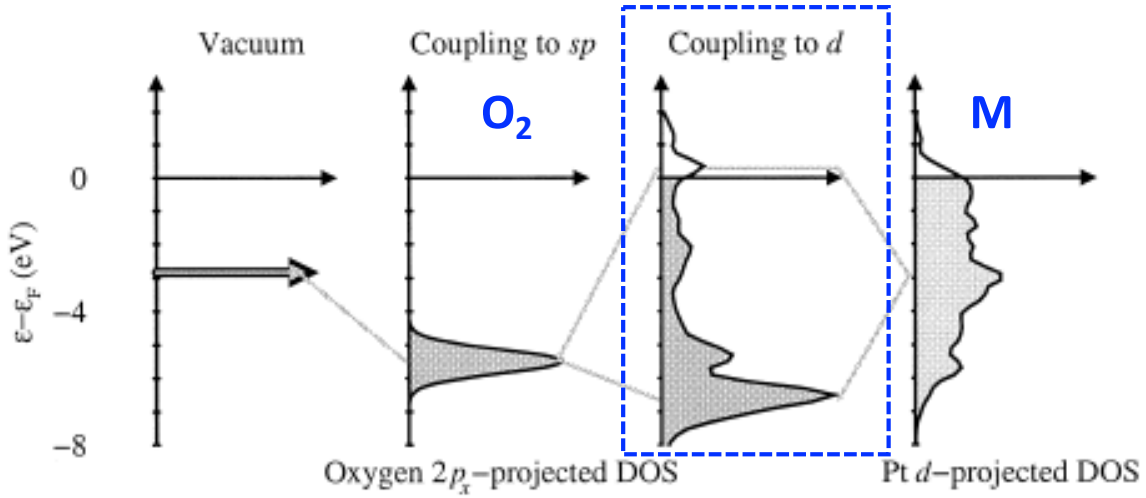

FIG. 8. Schematic illustration of the change in local electronic structure at an oxygen atom upon adsorption on simple and transition/noble metal surfaces. First, the sharp atomic states of the gas phase are broadened into resonances and shifted down due to the interaction with the metal *sp* states. Next, these renormalized states interact with the narrow *d* bands at the transition and noble metal surfaces, forming covalent bonding and antibonding states below and above the initial adsorbate and surface states. The coupling to the metal *d* electrons can roughly be viewed as a two-level coupling. The O/Pt(111) and Pt(111) DOS are from the self-consistent calculations in Fig. 7.

Adv. Catal. Vol. 45.

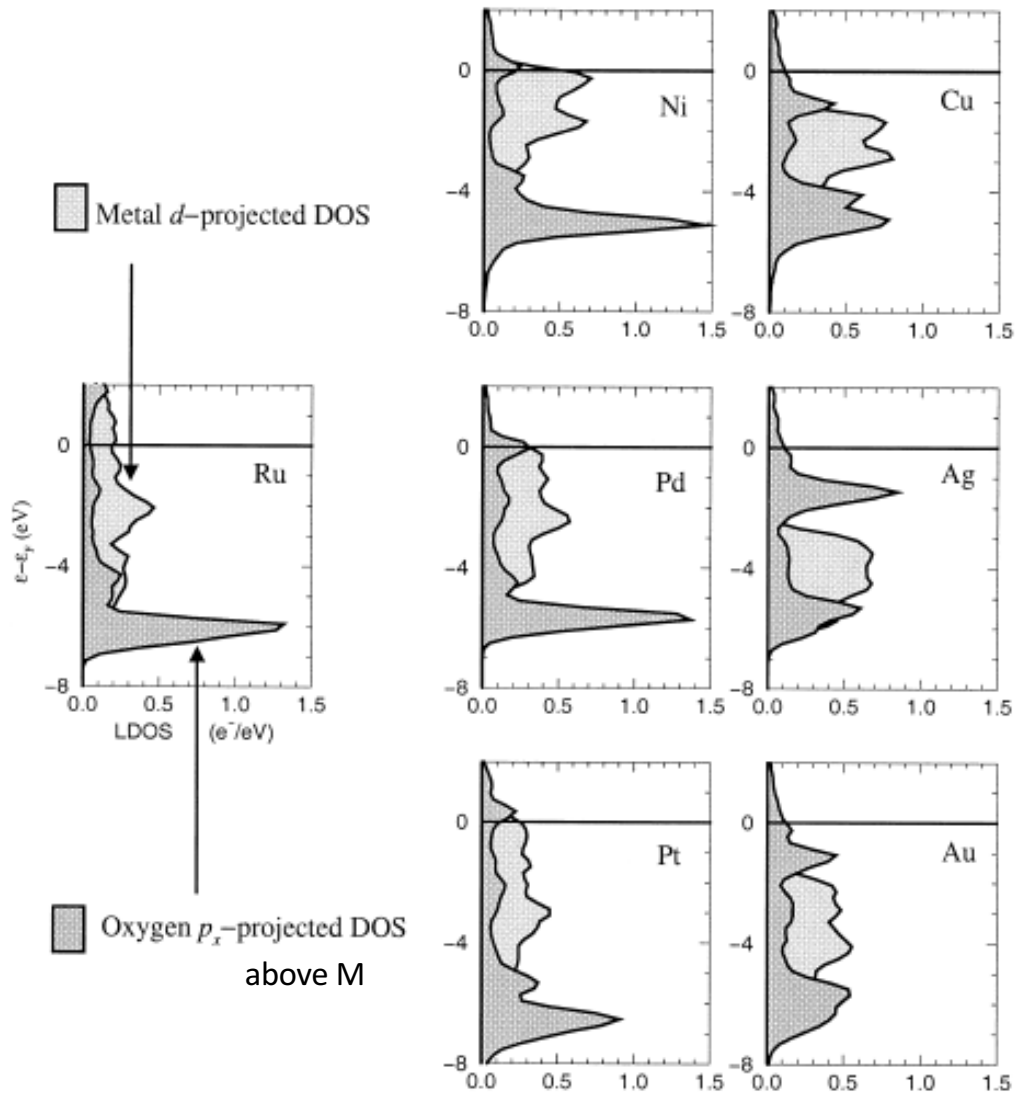

FIG. 7. Local density of states projected onto the oxygen $2p_x$ state (dark-shaded area) for atomic oxygen 1.3 Å above close-packed surfaces of late transition metals (cf. Fig. 6). The light-shaded areas give the metal *d*-projected DOS for the respective metal surfaces before the oxygen chemisorption. From Hammer and Nørskov (*40*).

***d* band center** is one possible measure of the reactivity of the transition metals.

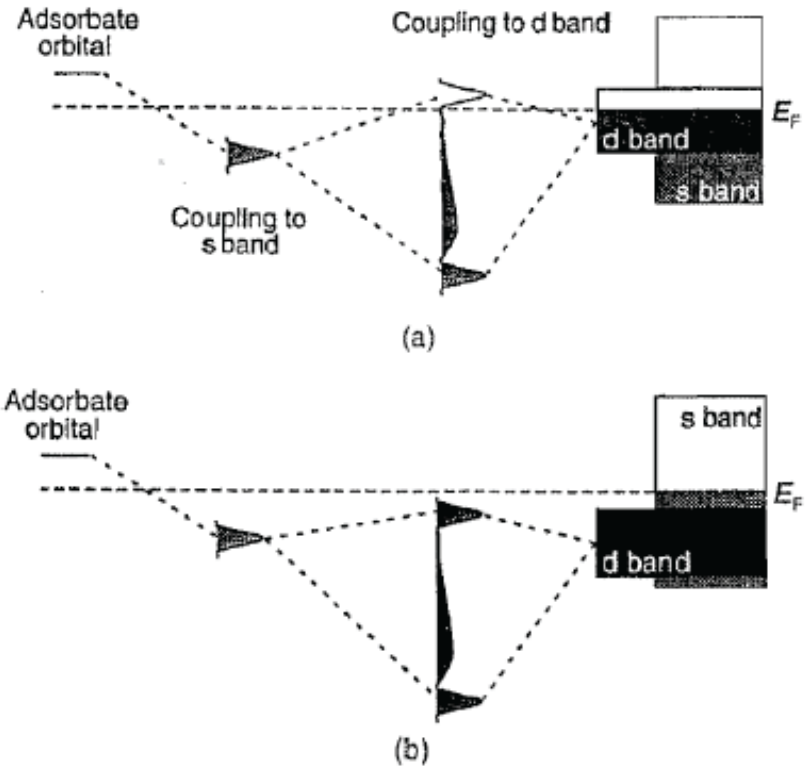

Filling of antibonding

Pauli repulsion (according to orbital overlap) for bonding (V^2_{ad})

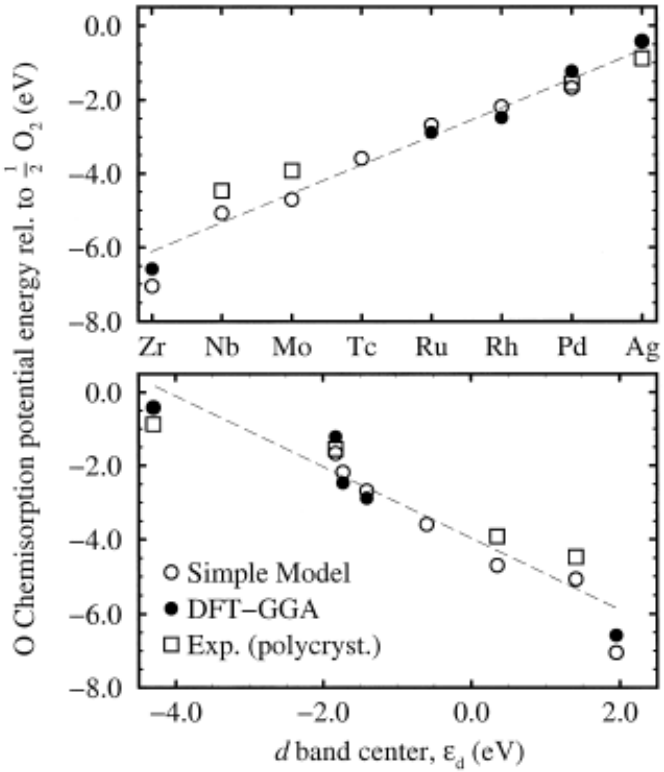

FIG. 9. Comparison of DFT-based oxygen chemisorption energies, E(O/surface) − $\frac{1}{2}E(O_2)$ − E (surface) (PW91), experimental values, and model estimates of the bond strengths for the various close-packed transition and noble metal surfaces. Data represented by open circles were determined by using the Newns–Anderson model. The experimental values are from Toyoshima and Somorjai (*49*). (Bottom) The calculated adsorption energies correlate well with the d band center ε_d.

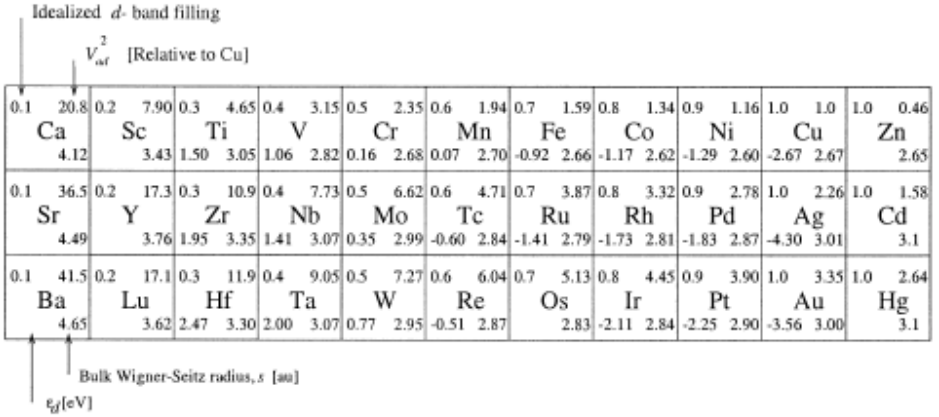

FIG. 10. Section of the periodic table with the 3*d*, 4*d*, and 5*d* transition metals. Shown in the lower right corner for each element is bulk Wigner–Seitz radius, s. In the lower left corner, the center of the d band is calculated for the most close-packed surface for each of the metals [(111) for fcc, (001) for hcp, and (110) for bcc]. In the upper right corner is shown the behavior of the adsorbate (s or p)–metal d-coupling matrix element squared, V^2_{ad}. The V^2_{ad}'s generally decrease for increasing nuclear charge within a row and increase down the groups. All the values, except for the properties of zinc, cadmium, and mercury were compiled from Andersen *et al.* (*50*). In the upper left corner, the idealized d band fillings are shown. These are similar to the actual, calculated bulk d band fillings considering the uncertainties in interpreting them (*50*).

3. ORR process

Origin of the Overpotential for Oxygen Reduction at a Fuel-Cell Cathode

J. K. Nørskov,* J. Rossmeisl, A. Logadottir, and L. Lindqvist

Center for Atomic-scale Materials Physics, Department of Physics, Technical University of Denmark, DK-2800 Lyngby, Denmark

ΔG_0	$\frac{1}{2}O_2 + * \rightarrow O*$ dissociation	(1)	$O_2 + * \rightarrow O_2*$
$\Delta G_1(rds)$	$O* + H^+ + e^- \rightarrow HO*$	(2)	$O_2* + (H^+ + e^-) \rightarrow HO_2*$
ΔG_2	$HO* + H^+ + e^- \rightarrow H_2O + *$	(3)	$HO_2* + (H^+ + e^-) \rightarrow H_2O + O*$

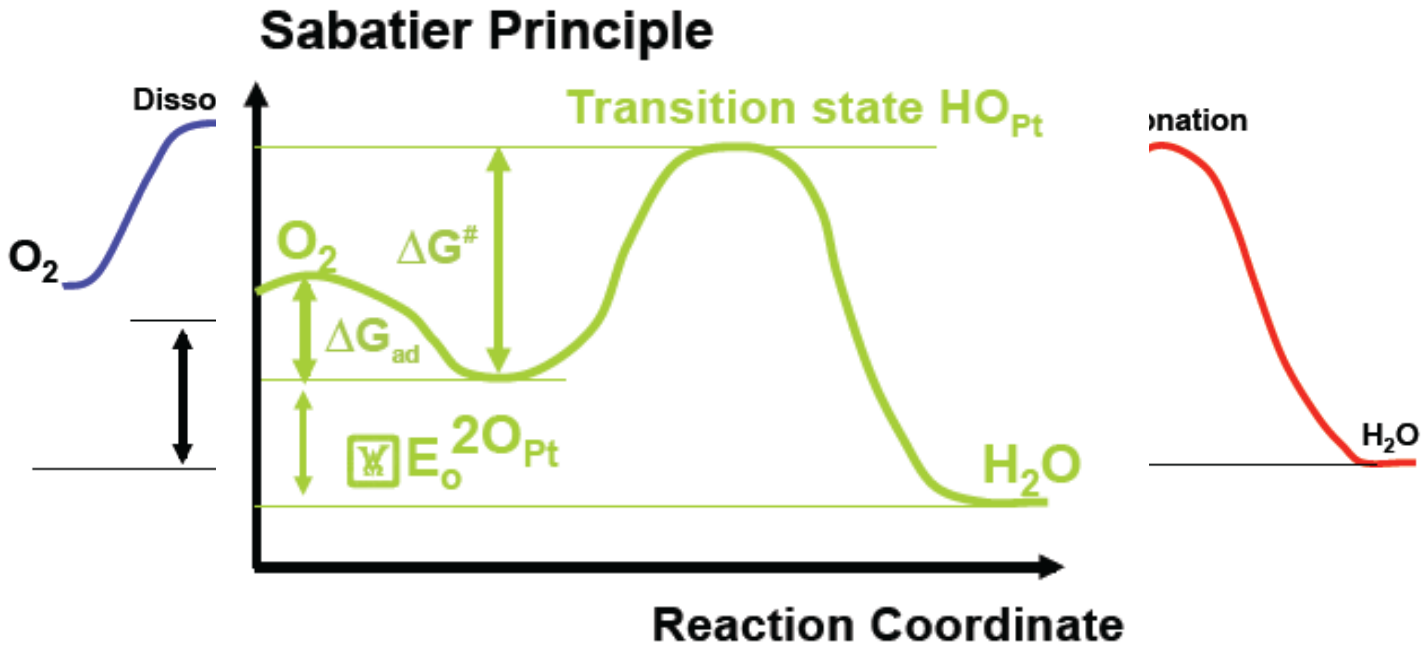

J. Phys. Chem. B. **2004**, *108*, 17886-17892.

3. ORR process

Origin of the Overpotential for Oxygen Reduction at a Fuel-Cell Cathode

J. K. Nørskov,* J. Rossmeisl, A. Logadottir, and L. Lindqvist

Center for Atomic-scale Materials Physics, Department of Physics, Technical University of Denmark, DK-2800 Lyngby, Denmark

ΔG_0 $\frac{1}{2}O_2 + * \rightarrow O^*$ ..... (1) ..... $O_2 + * \rightarrow O_2^*$

ΔG_1 $O^* + H^+ + e^- \rightarrow HO^*$ ..... (2) ..... $O_2^* + (H^+ + e^-) \rightarrow HO_2^*$

ΔG_2 $HO^* + H^+ + e^- \rightarrow H_2O + *$ ..... (3) ..... $HO_2^* + (H^+ + e^-) \rightarrow H_2O + O^*$

TABLE 2: Calculated Reaction Heats for Reaction 6 (ΔE_{OH}) and Reaction 7 (ΔE_O) over the Most Close Packed Surface of a Number of Metals at a Quarter Monolayer Coverage[a]

metal	ΔE_{OH} (eV)	ΔE_O (eV)	$\Delta G_0(U_0)$ (eV)	$\Delta G_1(U_0)$ (eV)	$\Delta G_2(U_0)$ (eV)	E_a^{diss} (eV)
Ag	0.72	2.12	−0.33	−0.43	0.76	0.93
Au	1.49	2.75	0.30	−0.29	−0.01	2.06
Co	−0.08	−0.22	−2.67	1.11	1.56	−3.29
Cu	0.37	1.20	−1.25	0.14	1.11	−0.73
Fe	−0.88	−0.90	−3.35	0.99	2.36	−4.51
Ir	0.63	1.00	−1.45	0.60	0.85	−1.09
Mo	−0.61	−1.62	−4.07	1.98	2.09	−5.81
Ni	0.13	0.34	−2.11	0.76	1.35	−2.28
Pd	0.92	1.53	−0.92	0.36	0.56	−0.14
Pt	1.05	1.57	−0.88	0.45	0.43	−0.06
Rh	0.34	0.44	−2.01	0.87	1.14	−2.10
Ru	−0.01	−0.05	−2.50	1.01	1.49	−2.98
W	−0.80	−2.06	−4.51	2.23	2.28	−6.60

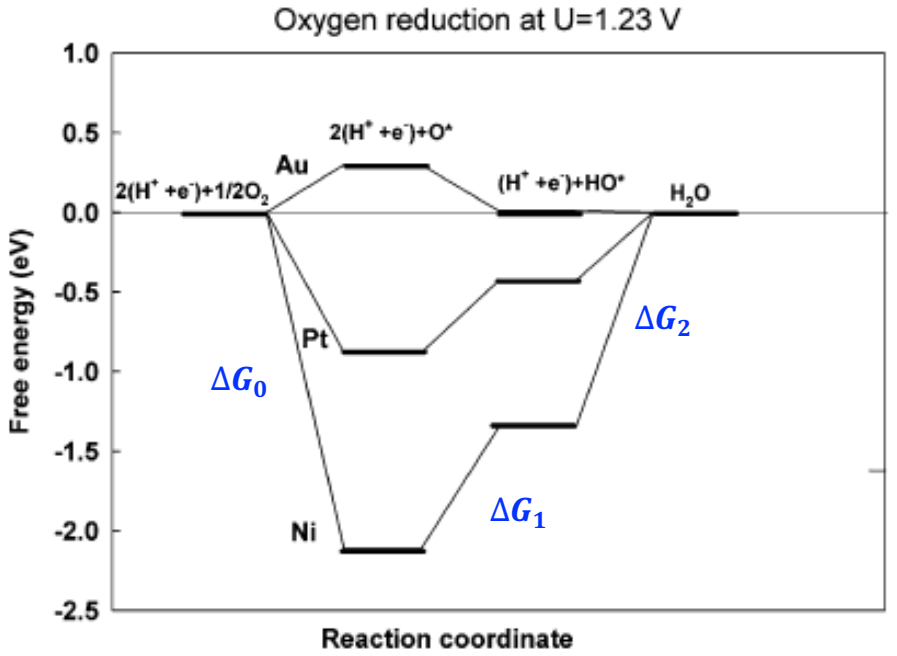

Figure 3. Free-energy diagram for oxygen reduction at the equilibrium potential $U_0 = 1.23$ V over Pt, Au, and Ni.

J. Phys. Chem. B. **2004**, *108*, 17886-17892.

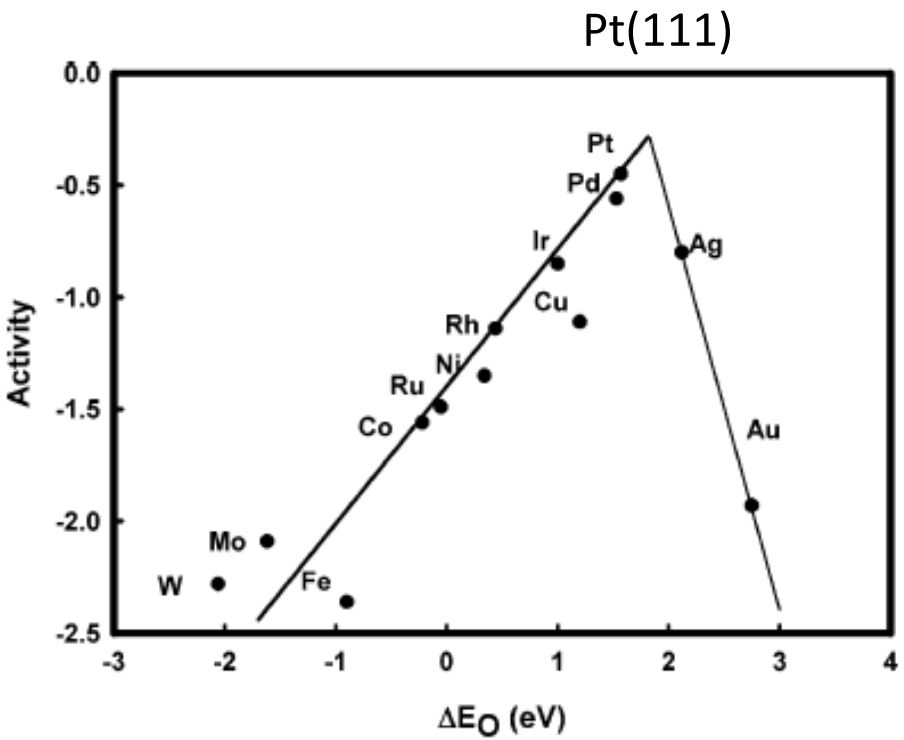

Figure 4. Trends in oxygen reduction activity (defined in the text) plotted as a function of the oxygen binding energy.

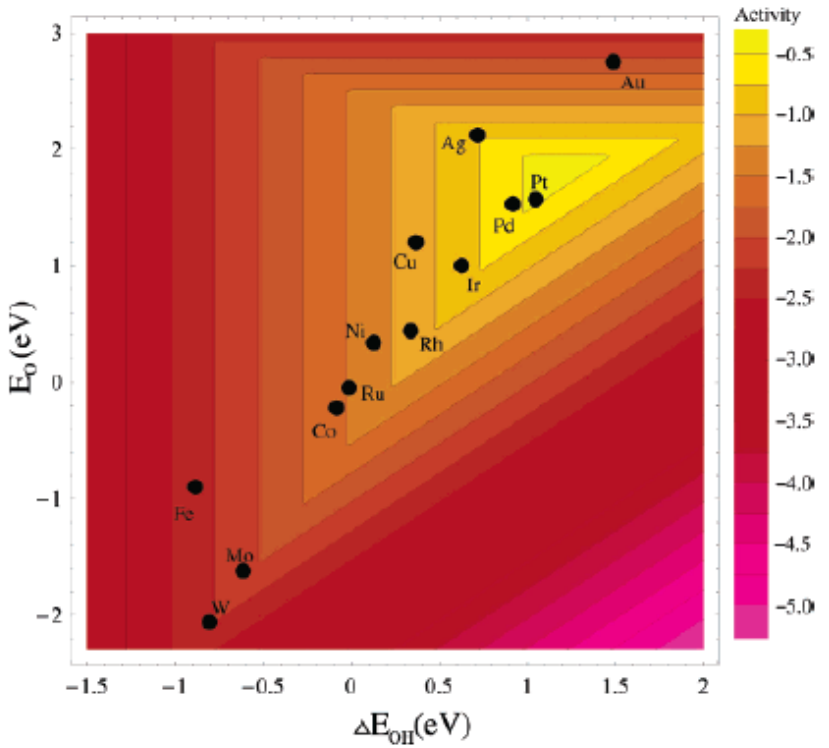

Figure 5. Trends in oxygen reduction activity plotted as a function of both the O and the OH binding energy.

- Origin of the η for Pt: Pt(111) as electrode adsorbed oxygen tends to be so stable at high potentials that the H^+ and e^- transfer becomes impossible. By lowering the potential, the stability of oxygen decreases and the rxn may proceed.
- The total process is highly dependent on the *metal (electrocatalyst) and potential (including the bias dependence of the oxygen coverage and the coverage-dependent oxygen adsorption energy)*.
- The Pt-oxygen bonding is still very high: lower oxygen binding energy than Pt should have a higher rate of ORR (e.g. Pt alloys).

4. Electrochemical results

Acidic solns

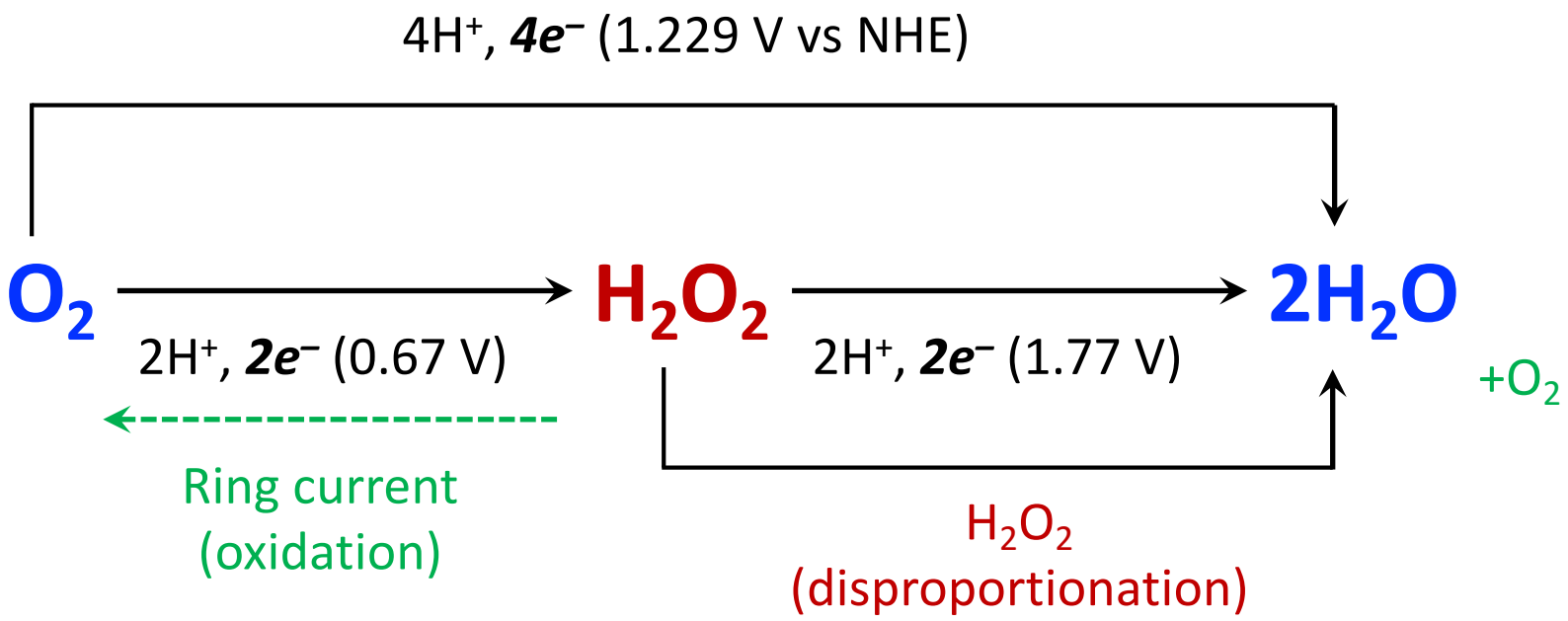

- Dissociation energy of O=O bond: 494 kJ/mol
- Dissociation energy of HO–OH bond: 146 kJ/mol

$$O_2 + * \rightarrow O_2*$$

$$O_2* + (H^+ + e^-) \rightarrow HO_2*$$

$$HO_2* + (H^+ + e^-) \rightarrow HO_2*H \rightarrow H_2O_2?$$

$$HO_2* + (H^+ + e^-) \rightarrow 2(HO)* + 2(H^+ + e^-) \rightarrow 2H_2O$$

$$HO_2* + (H^+ + e^-) \rightarrow O* + H_2O + 2(H^+ + e^-) \rightarrow H_2O$$

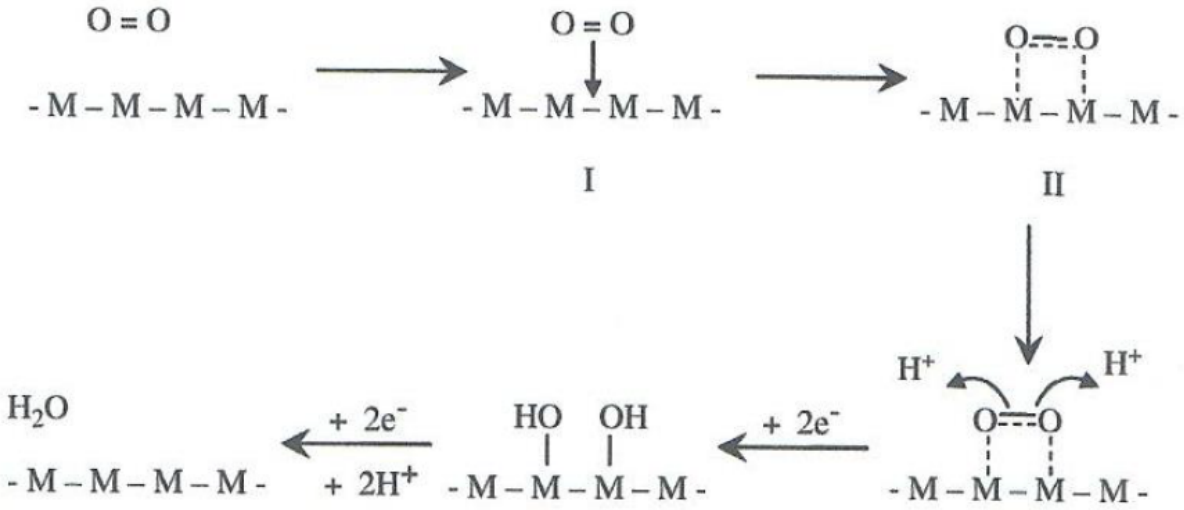

Polycrystalline Pt disk|acidic solution (1 M $HClO_4$)|Ar|10 mV/s

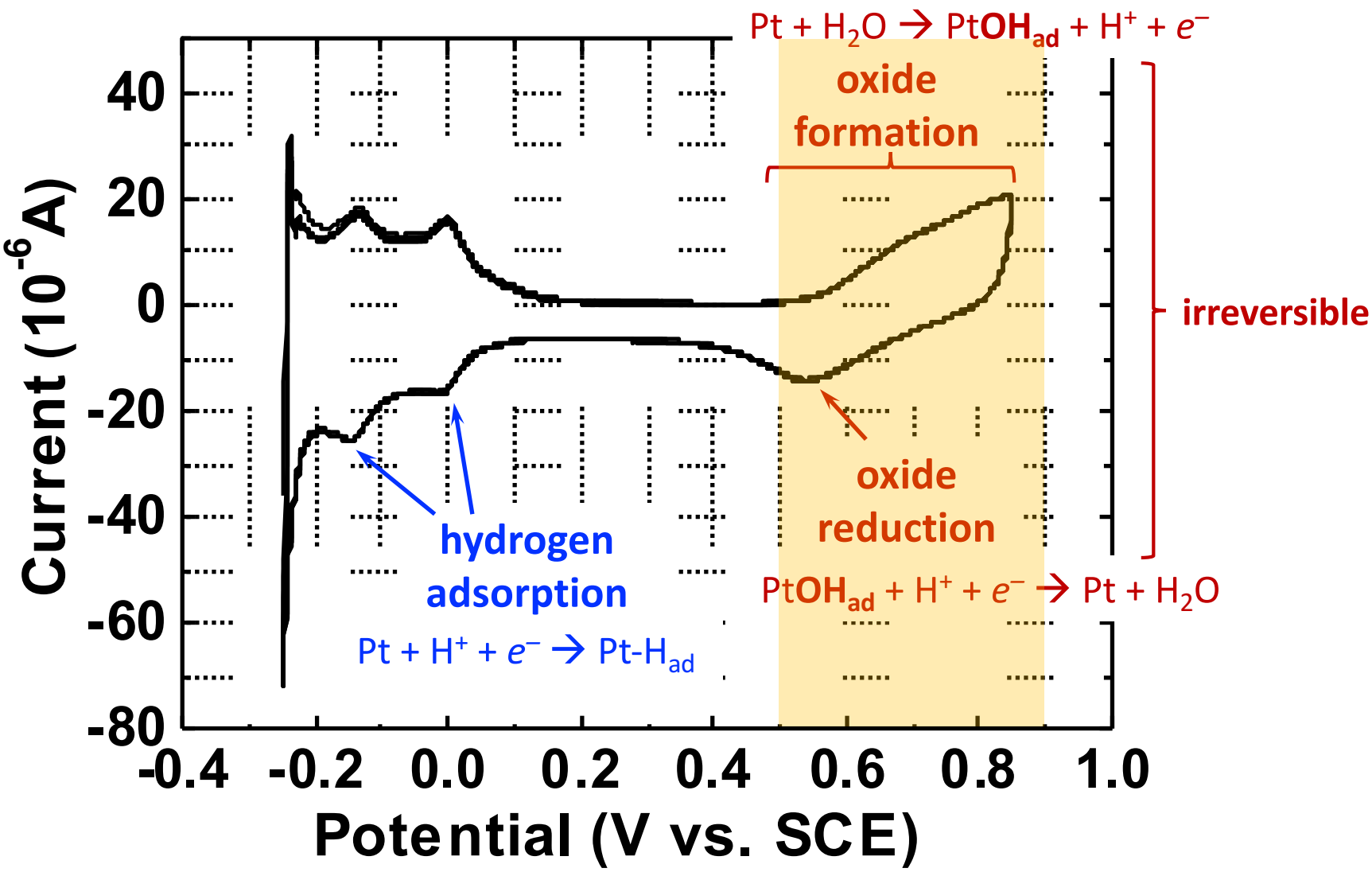

- Oxygen adsorption vs. OH coverage (low η)
- Oxygen adsorption vs anion coverage (middle η)
- Oxygen adsorption vs. H coverage (high η)

H_{upd}, OH_{ads}, $anion_{ads}$ are not involved in the ORR!

• RRDE system : measurement of intermediates

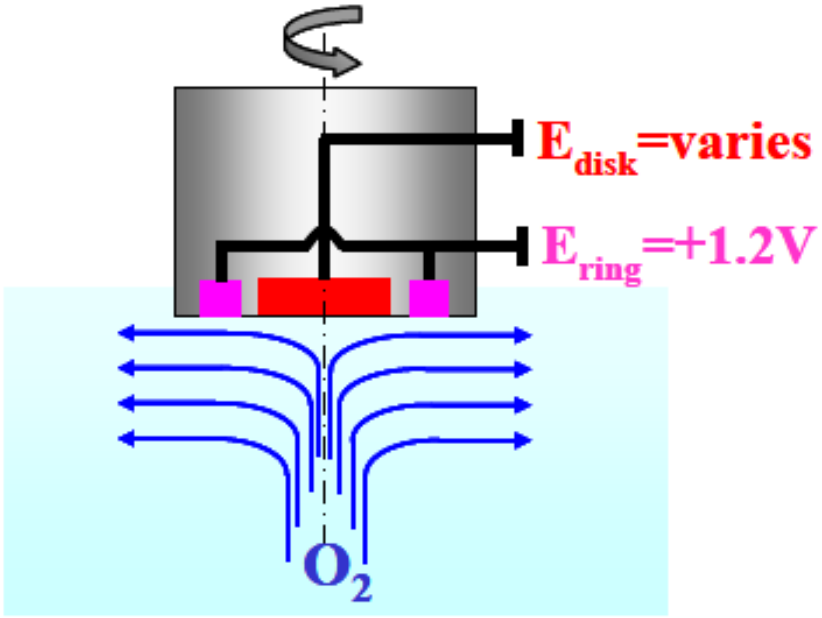

e.g. ORR proceeds either to H_2O_2 (2-electron path) or H_2O (4-electron path):

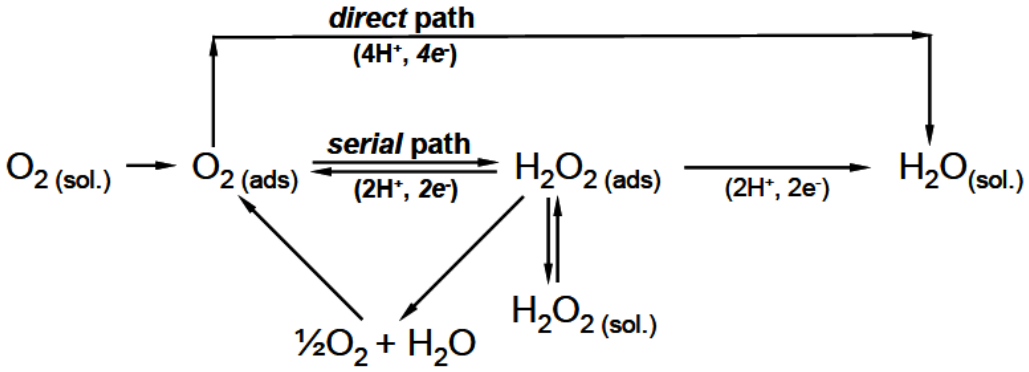

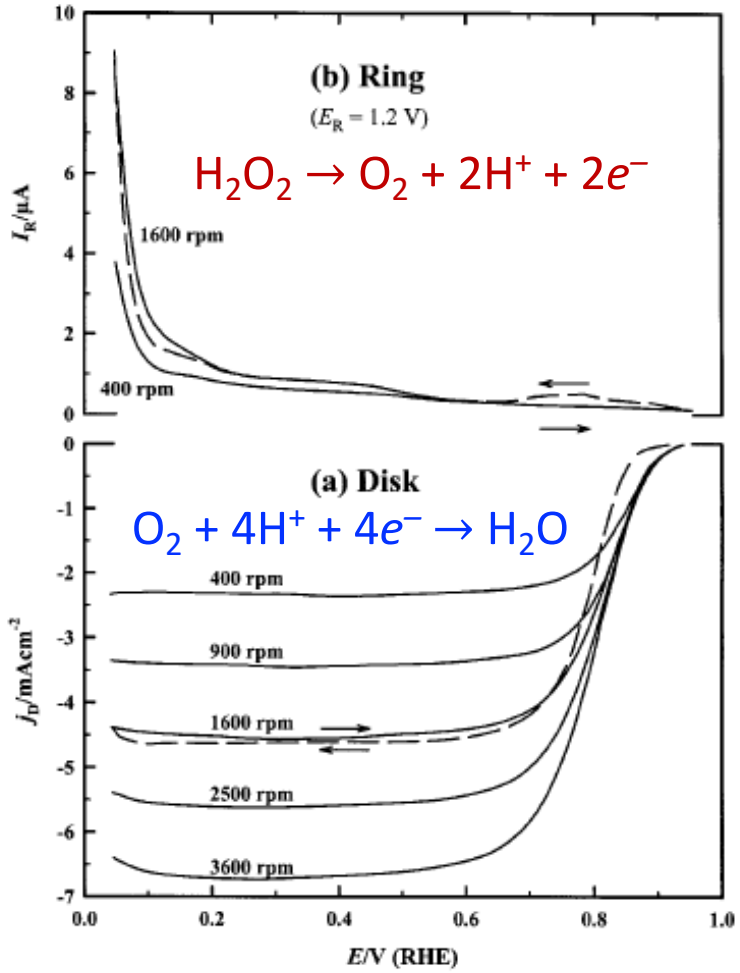

Fig. 4. (a) Potentiodynamic (5 mV s^{-1}, positive sweep) O_2 reduction current densities (j_D) on a thin-film RRDE with Pt/Vulcan catalyst (14 μg_{Pt} cm^{-2}) at 60°C in 0.5 M H_2SO_4 saturated with 1 bar O_2. (b) Simultaneously recorded ring currents (I_R) at 400 and 1600 rpm for a ring potential of $E_R = 1.2$ V. The dashed lines show the negative going sweeps at 1600 rpm.

J. Electroanalytical Chem. **2001**, *495*, 134-145.

Oxygen Reduction on Platinum Low-Index Single-Crystal Surfaces in Sulfuric Acid Solution: Rotating Ring−Pt(*hkl*) Disk Studies

Nenad M. Marković,* Hubert A. Gasteiger, and Philip N. Ross, Jr.

Materials Science Division, Lawrence Berkeley Laboratory, Berkeley, California 94720

Received: September 28, 1994; In Final Form: December 16, 1994®

0.05 M H_2SO_4

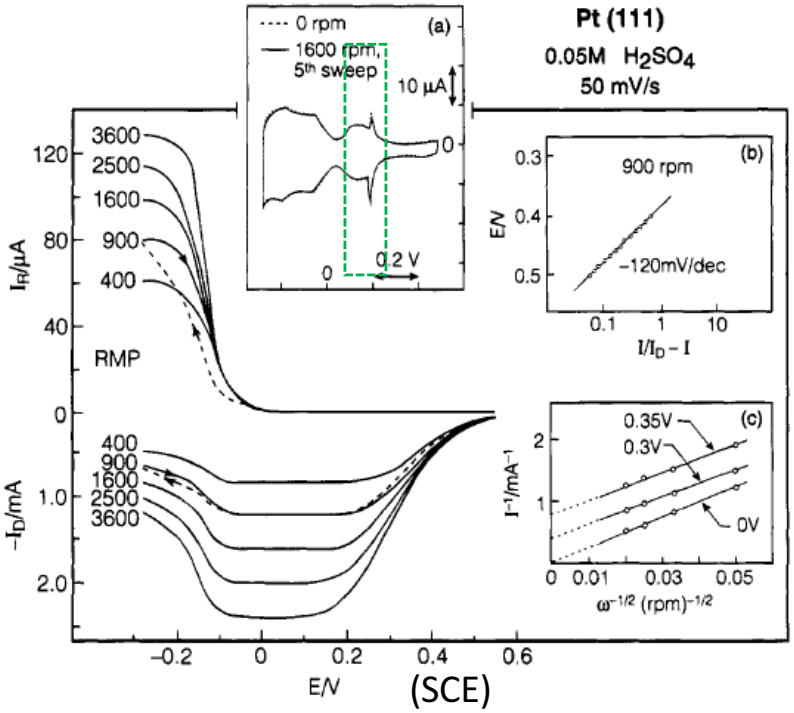

- I_k: Pt(110) > Pt(100) > Pt(111)
- n = 4
- For Pt(111) and Pt (100): (bi)sulfate adsorption blocks the initial adsorption of O_2 (middle η).
- For Pt(100) and (110): (small) OH_{ads} effect for the initial adsorption of O_2 (low η).

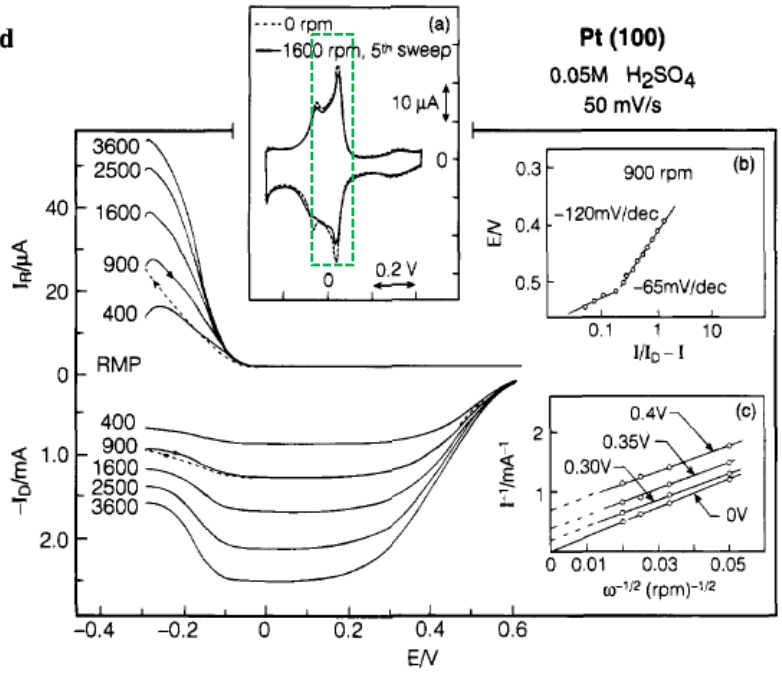

2. Disk (I_D) and ring (I_R) currents during oxygen reduction on Pt(100) in 0.05 M H_2SO_4 at a sweep rate of 50 mV/s (ring potential = 0.95) positive-going sweeps; (- - -) negative-going sweep at 900 rpm. (a) Cyclic voltammetry of Pt(100) in the RRDE assembly in oxygen-free yte with and without rotation. (b) Tafel plot at 900 rpm. (c) Levich plot at various electrode potentials.

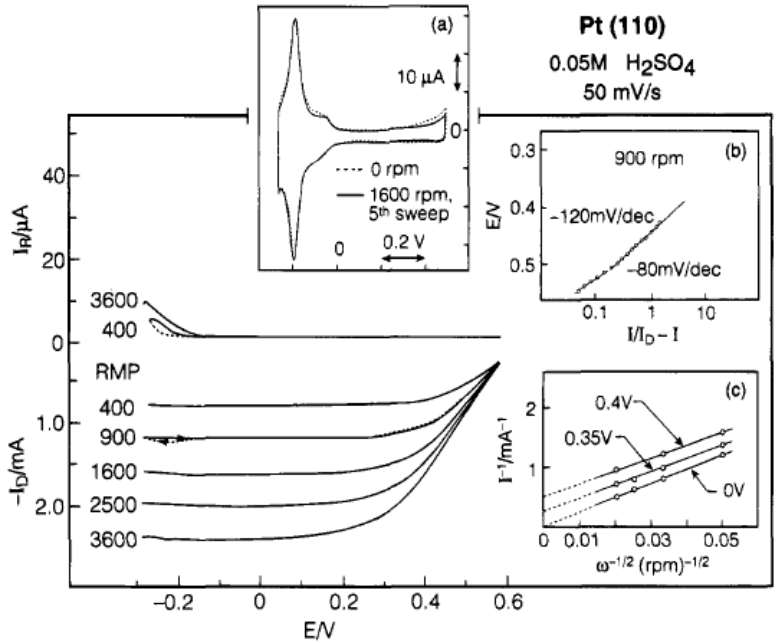

Figure 3. Disk (I_D) and ring (I_R) currents during oxygen reduction on Pt(110) in 0.05 M H_2SO_4 at a sweep rate of 50 mV/s (ring potential = 0.95 V): (—) positive-going sweeps; (- - -) negative-going sweep at 900 rpm. (a) Cyclic voltammetry of Pt(110) in the RRDE assembly in oxygen-free electrolyte with and without rotation. (b) Tafel plot at 900 rpm. (c) Levich plot at various electrode potentials.

J. Phys. Chem. **1995**, *99*, 3411-3415.

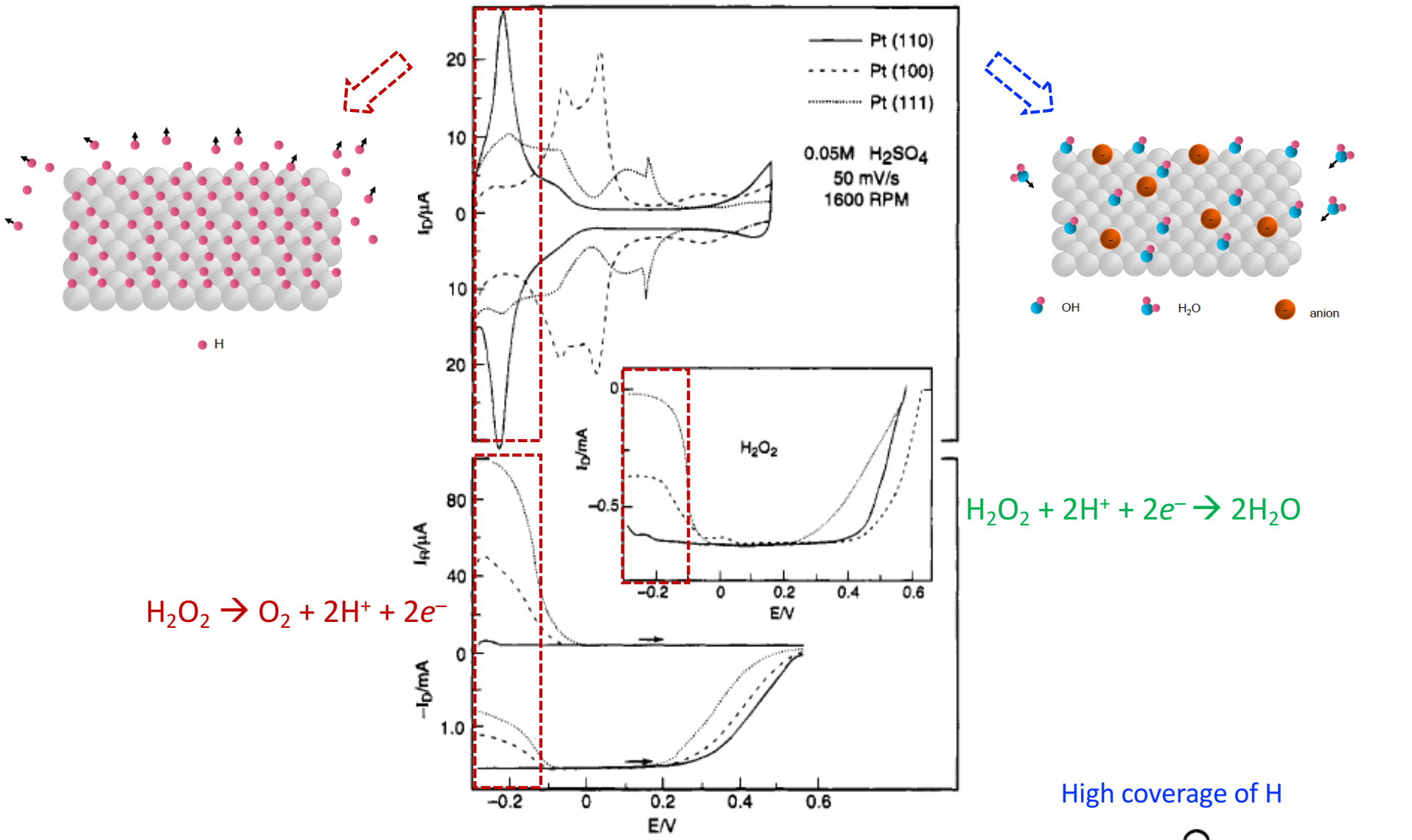

Figure 4. Top: cyclic voltammetry of Pt(*hkl*) in oxygen-free electrolyte in the RRDE assembly (fifth sweep). Bottom: disk (I_D) and ring (I_R) currents during oxygen reduction on Pt(*hkl*) (ring potential = 0.95 V). Insert: reduction of 1.2×10^{-3} M H_2O_2 on Pt(*hkl*) mounted in the RRDE assembly (0.05 M H_2SO_4, 50 mV/s, 1600 rpm).

High coverage of H

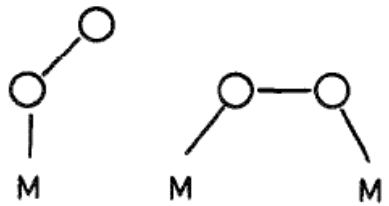

The deactivation by **H_{upd}** is entirely due to a **loss of adsorption sites which break the O–O bond** and not due to an interaction of O_2 and H_{upd}(high η). ➔ H_{upd} is not involved in the ORR.

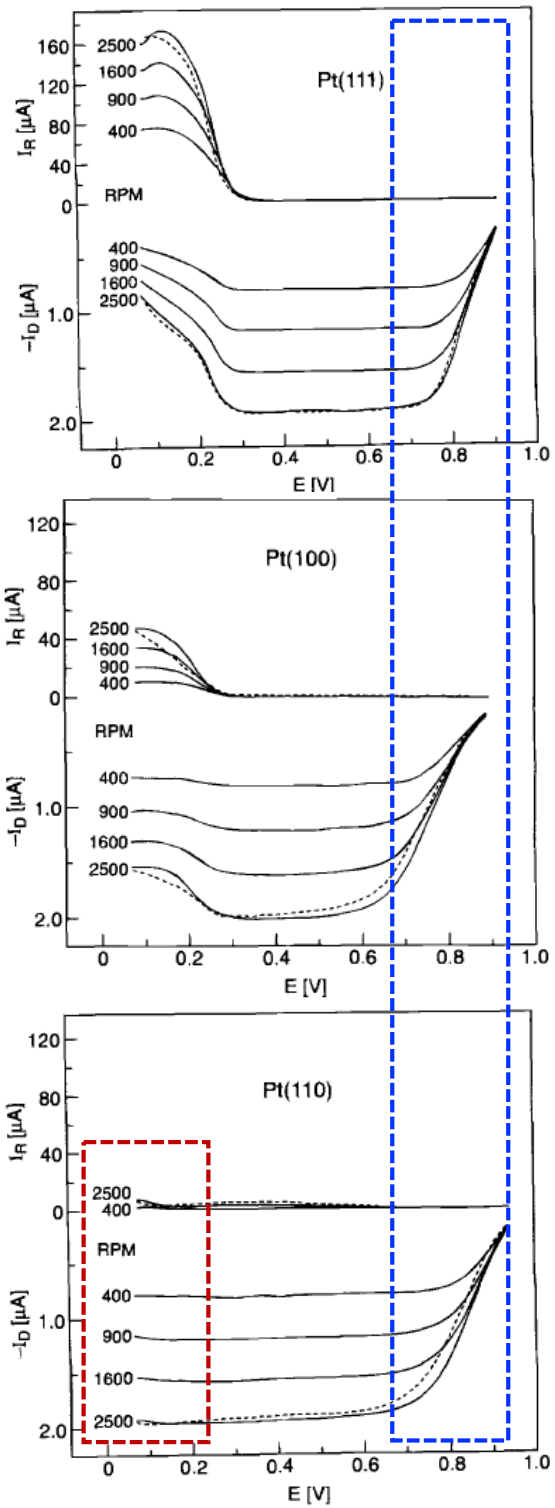

0.1 M $HClO_4$ **Pt(111) > Pt(110) > Pt(100)**

No blocking effect of anion

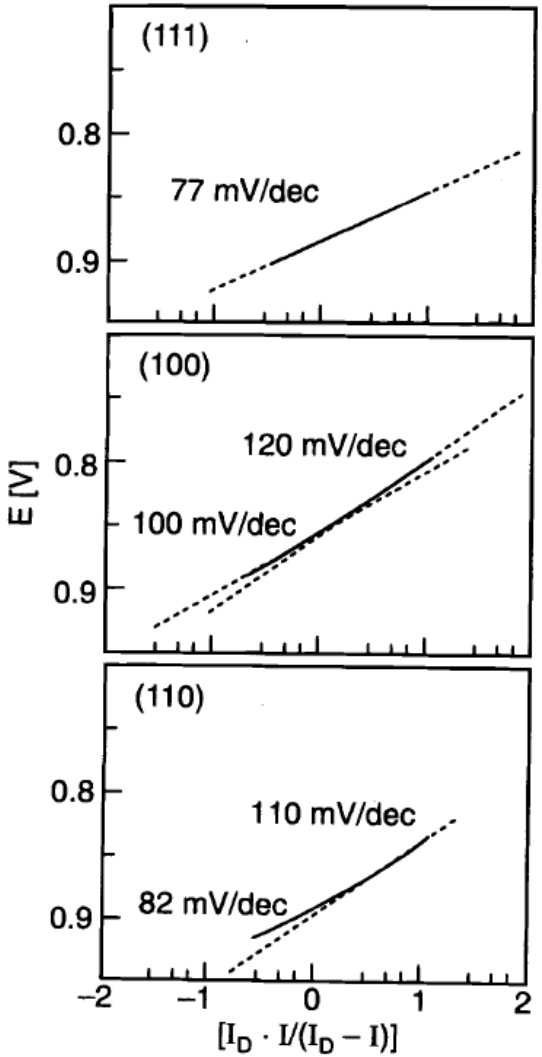

Fig. 4. Tafel plots of the Pt(hkl) disk currents at 900 rpm in oxygen saturated 0.1 *M* $HClO_4$ corrected for mass-transfer resistance.

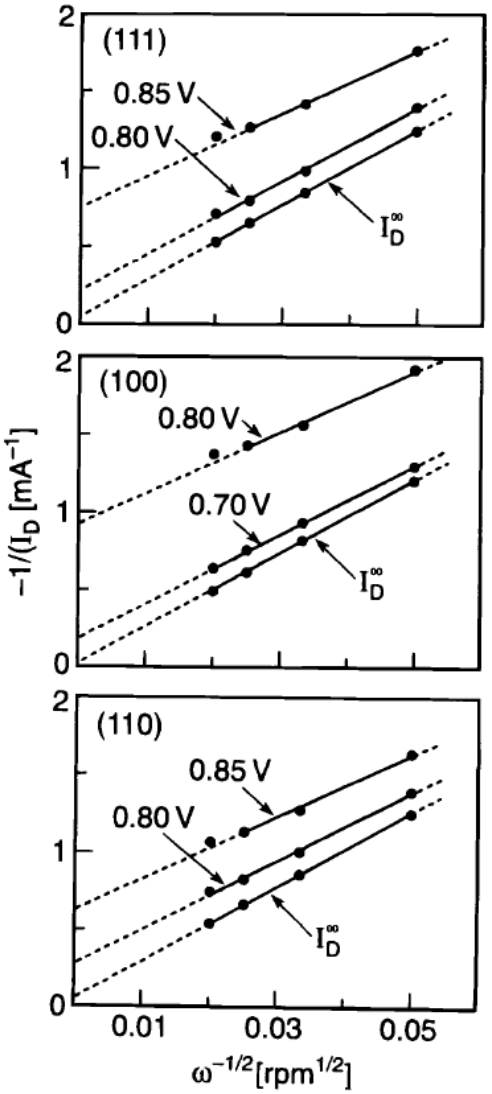

Fig. 5. Levich-Koutecky plots of the Pt(hkl) disk currents in oxygen saturated 0.1 *M* $HClO_4$ to determine kinetic currents at different potentials.

For Pt(110), H_{upd} and O–O bond dissociation may take place on different sites on the surface.

J. Electrochem. Soc. **1997**, *144*, 1591-1597.

In alkaline sol'n

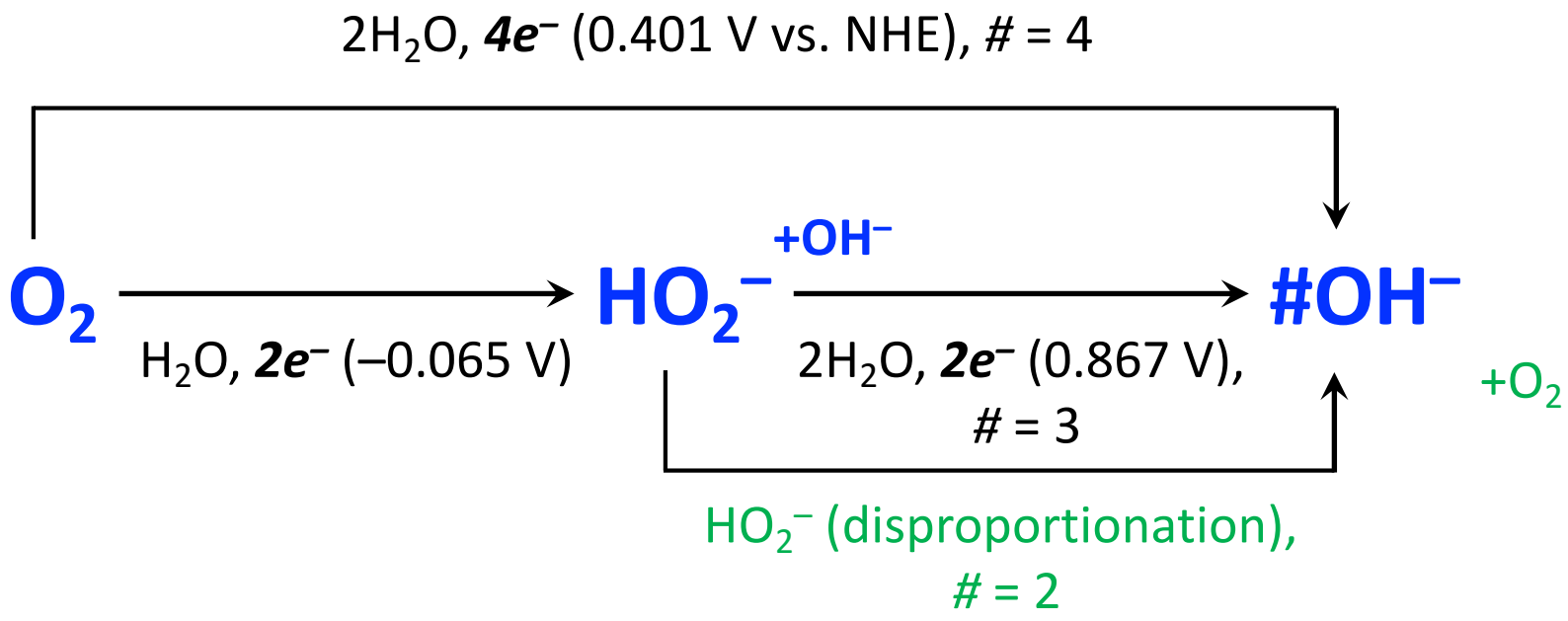

0.1 M KOH

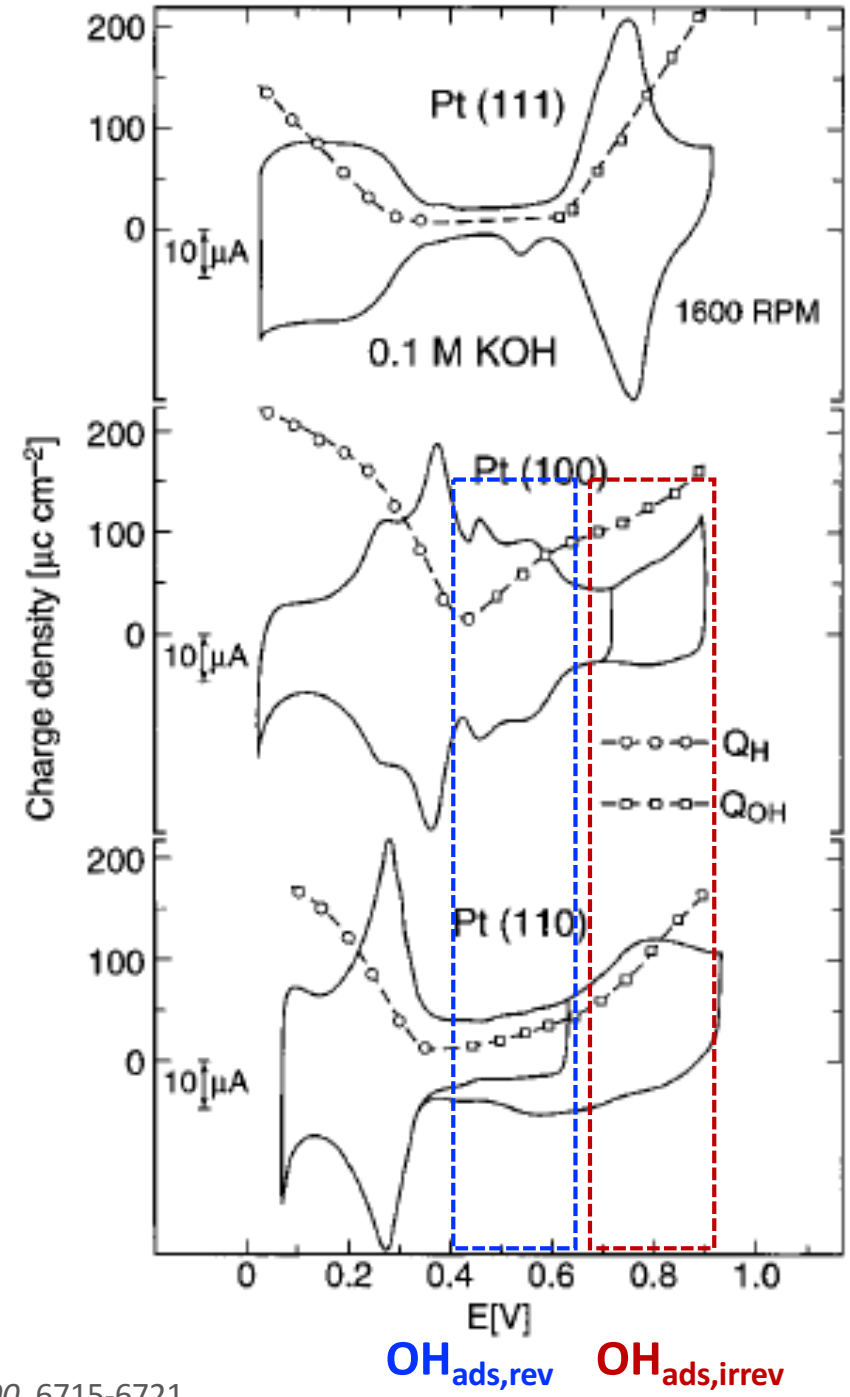

- In alkaline,
  $OH^- \leftrightarrow OH_{ads,rev} + 1e^-$
  $OH^- \rightarrow OH_{ads,irrev} + 1e^-$

- $OH_{ads,irrev}$ form is stronger, suggesting cooperative effects associated with a 2-D adlayer. (much thicker than that in acidic sol'n)

- **OH_{ads} is an inhibiting species for the ORR**, which is very different from small effect of OH_{ads} in acidic sol'n ($H_2O \rightarrow OH_{ads} + H^+ + 1e^-$, little effect for ORR, ½ coverage of OH_{ads} in alkaline sol'n)

J. Phys. Chem. **1996**, *100*, 6715-6721.

0.1 M KOH

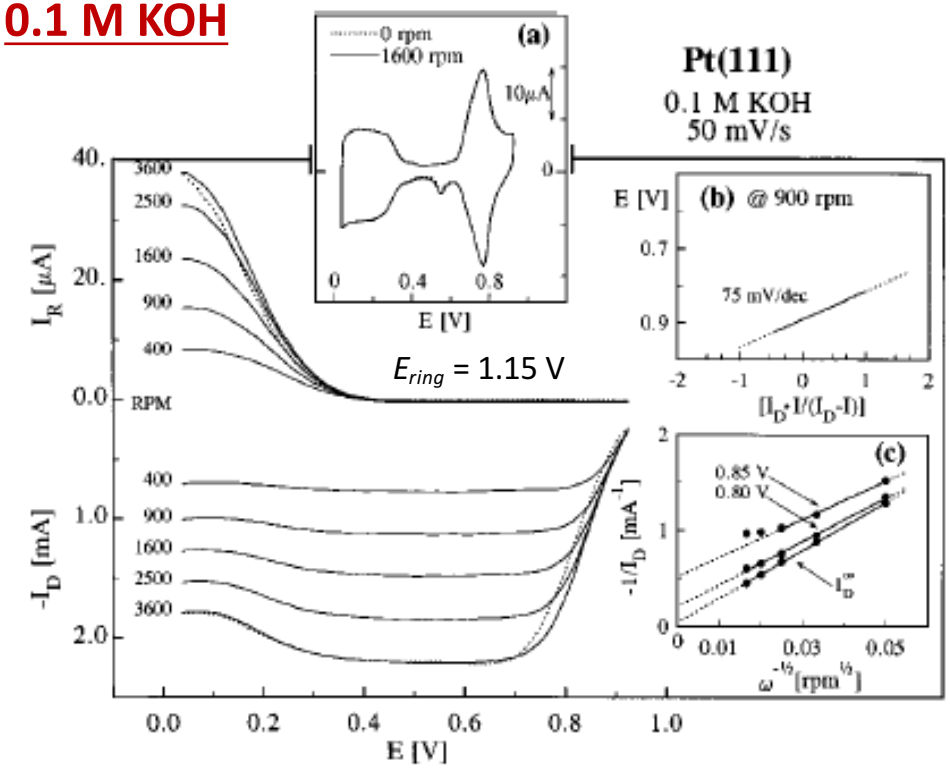

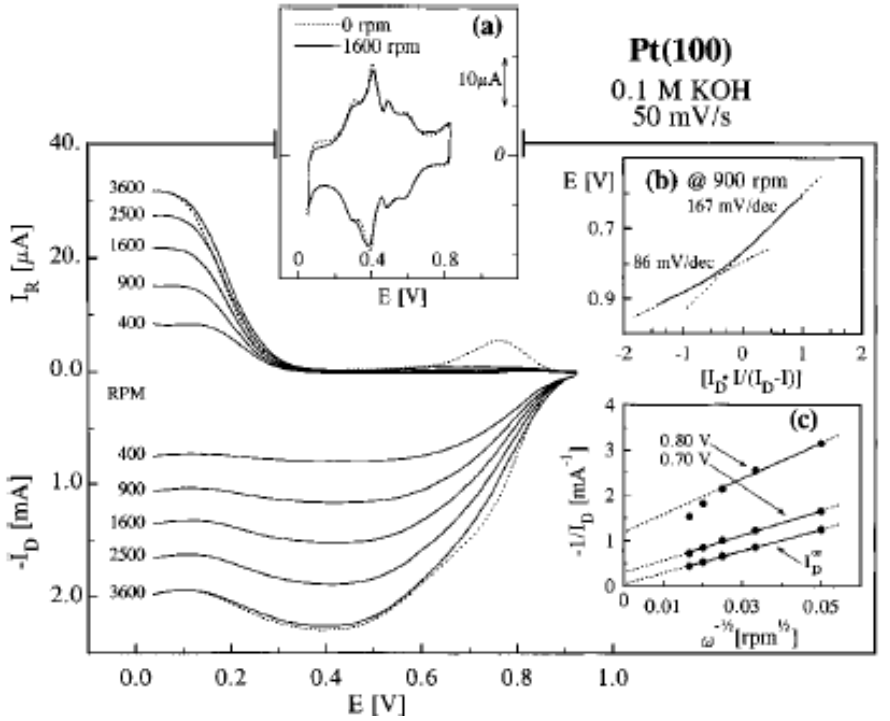

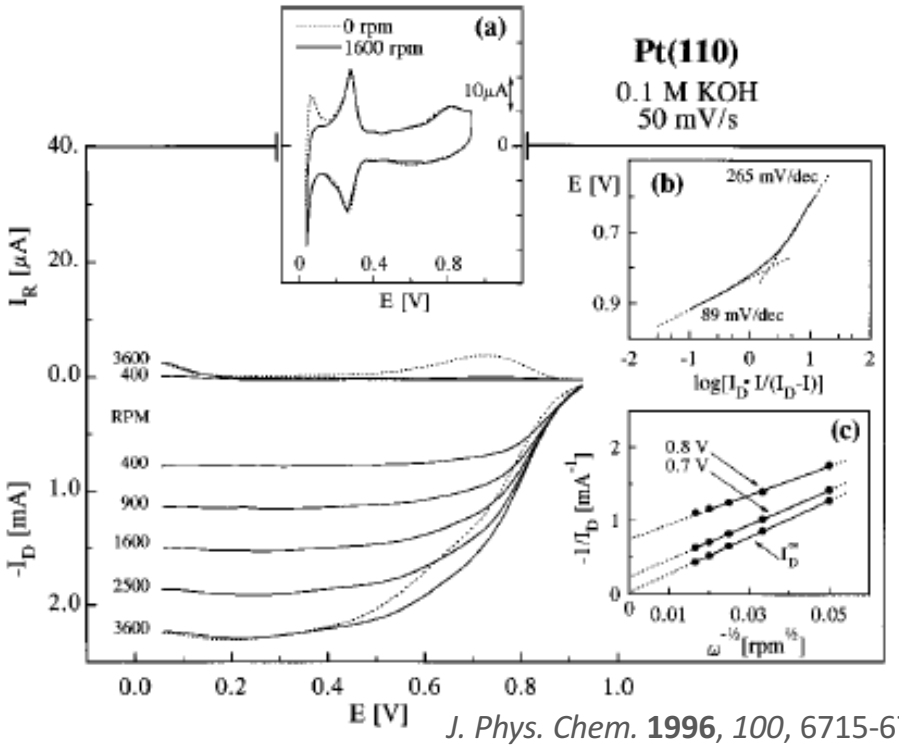

- I_k: Pt(111) > Pt(110) > Pt(100)
- n = 4
- For Pt(100) and (110): OH_{ads} effect for the initial adsorption of O_2 (low η).
- Reversible and irreversible OH_{ads} affects the ORR: A reversible **OH_{rev}** species only effect on the initial adsorption of O_2, **OH_{irrev}** affects both the initial adsorption of O_2 and the rxn mechanism (formation of H_2O_2 at negative potential sweeping at low η).
- Also H_{upd} effect (high η) is similar to in acidic sol'n.

J. Phys. Chem. **1996**, *100*, 6715-6721.

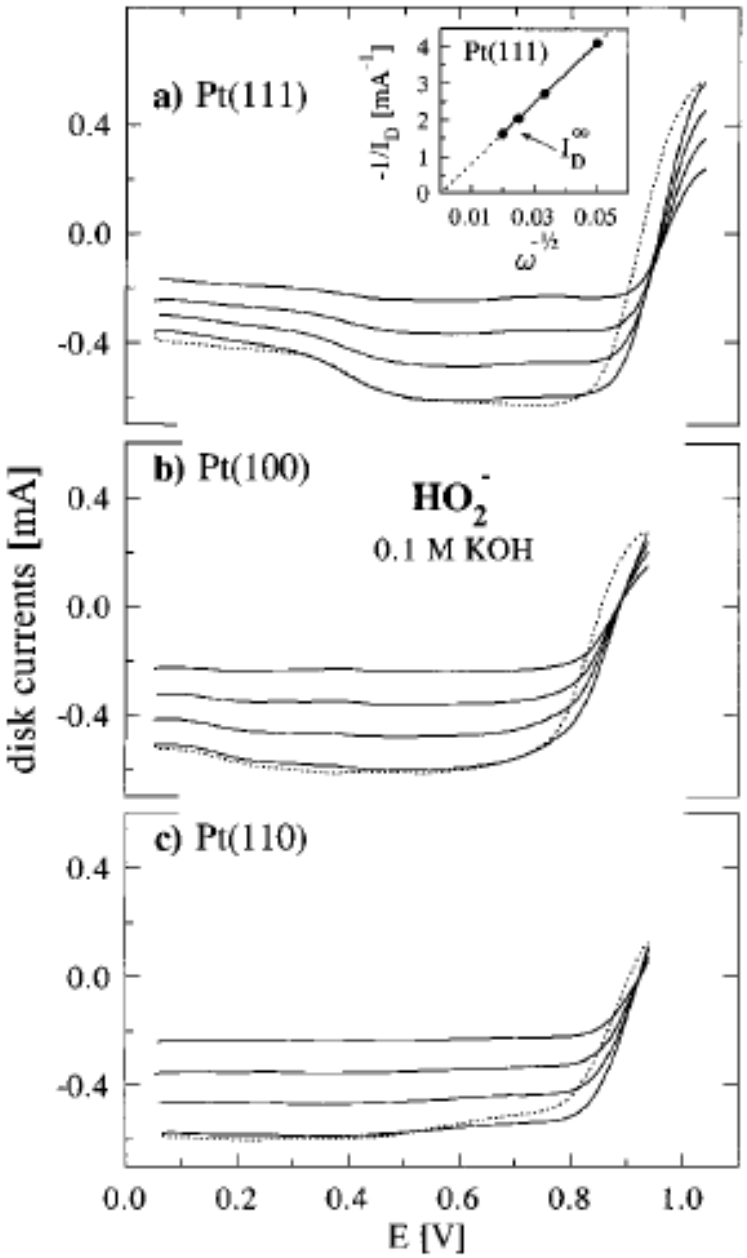

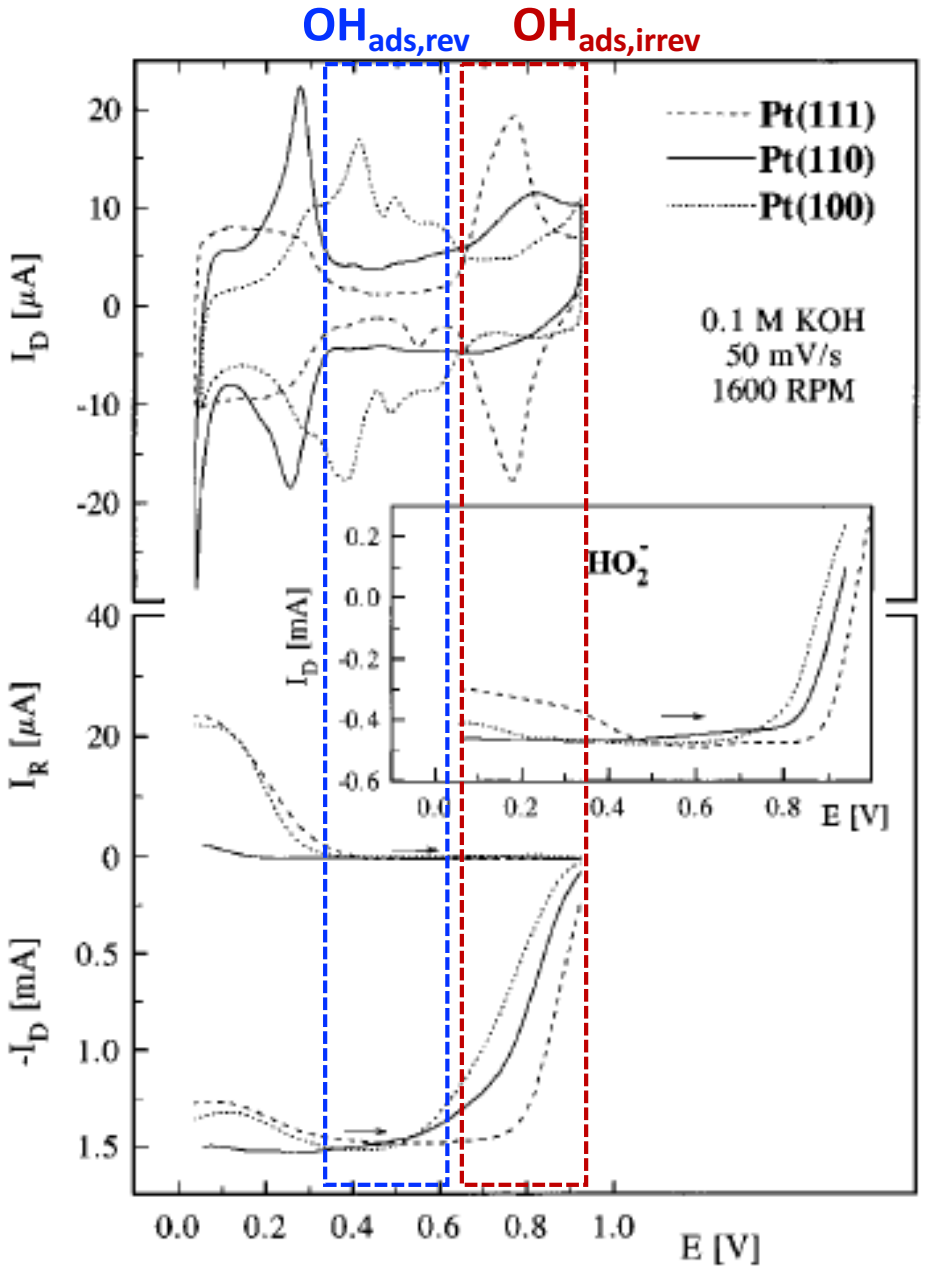

○ ORR activity order = peroxide activity order

○ *n* = 2

○ **OH_{ads} is an inhibiting species for the ORR**.

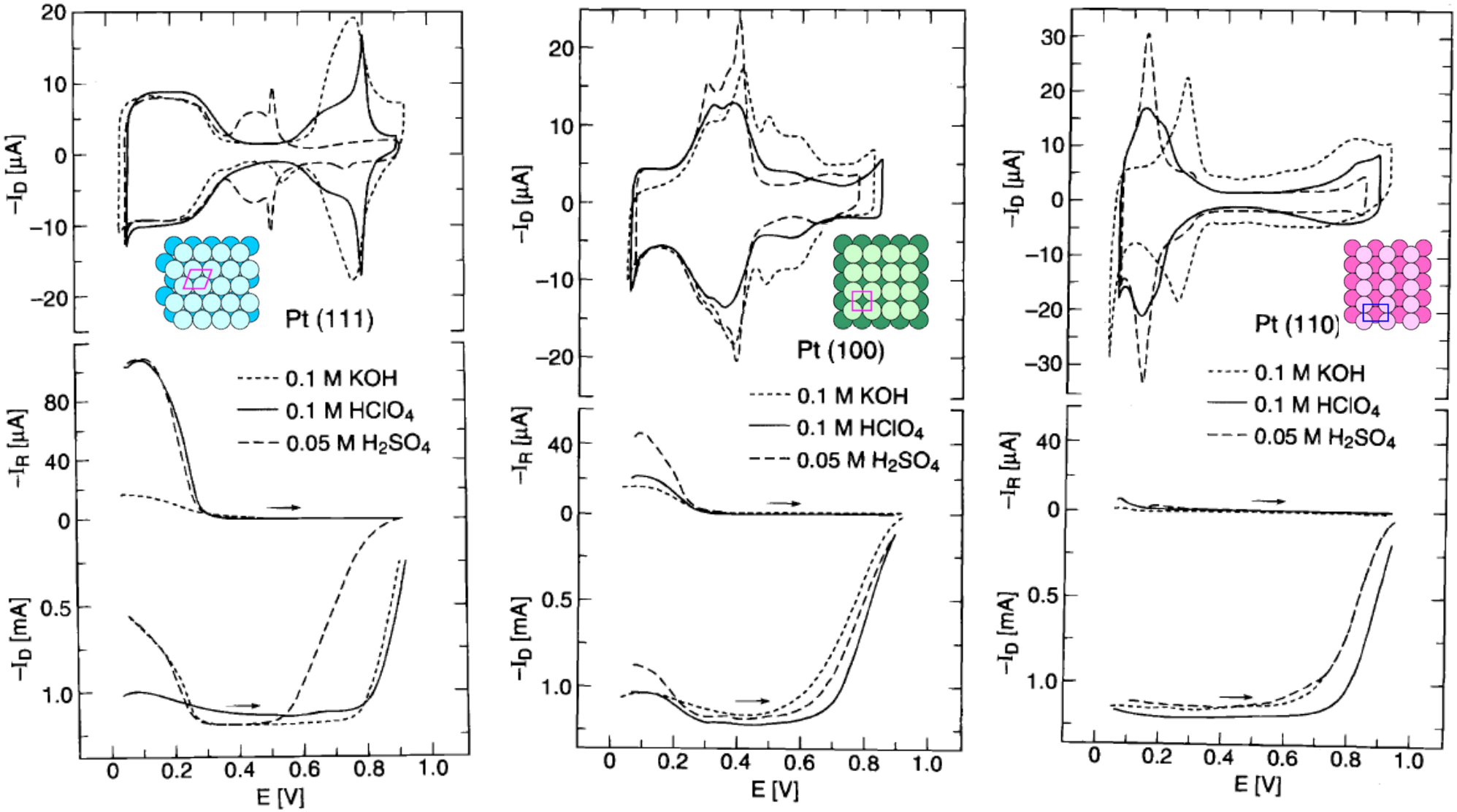

0.1 M $HClO_4$ Pt(111) > Pt(110) > Pt(100)

0.05 M H_2SO_4 Pt(110) > Pt(100) >> Pt(111)

0.1 M KOH Pt(111) > Pt(110) > Pt(100)

J. Electrochem. Soc. **1997**, *144*, 1591-1597.